Effect of the Variable Kuroshio Intrusion Pathway on Deep Flow in the Northern South China Sea

QI QUAN,[a,b] HAN ZHANG,[b,c,d] XIAOHUI LIU,[b,c] YI YU,[b] YANG YANG,[d] QINGYOU HE,[e] AND YA PING WANG[a]

[a] *State Key Laboratory of Estuarine and Coastal Research, East China Normal University, Shanghai, China*
[b] *State Key Laboratory of Satellite Ocean Environment Dynamics, Second Institute of Oceanography, Ministry of Natural Resources, Hangzhou, China*
[c] *Southern Marine Science and Engineering Guangdong Laboratory (Zhuhai), Zhuhai, China*
[d] *State Key Laboratory of Marine Environmental Science, and Department of Physical Oceanography, College of Ocean and Earth Sciences, Xiamen University, Xiamen, China*
[e] *State Key Laboratory of Tropical Oceanography, and Guangdong Key Laboratory of Ocean Remote Sensing, South China Sea Institute of Oceanology, Chinese Academy of Sciences, Guangzhou, China*

(Manuscript received 27 May 2024, in final form 13 September 2024, accepted 21 October 2024)

ABSTRACT: The effect of the variable Kuroshio intrusion pathway on deep flow in the northern South China Sea (NSCS) is investigated using observational and theoretical analyses. With significant seasonality in path variation, the leaking path is found to be most frequent, whereas the looping (leaping) path is transient and prefers to occur in winter (summer). Such multipath variability contributes greatly to the highest surface eddy kinetic energy in the NSCS, with the energy peaking for the looping path in winter, followed by the leaking and leaping paths. The information flow–based causality analysis suggests that the energetic surface perturbations in the Kuroshio intrusion region are causal to the intraseasonal variability in deep flow east of the Dongsha Islands, wherein the linkage is strongest within the Kuroshio Loop Current eddy shedding event related to the looping path. Therefore, the underlying dynamics for the vertical coupling is illustrated by this event, in which the eddy is highly compressed to the surface because of sloping topography and its energy is partially transferred downward through vertical pressure work to force the abyssal topographic Rossby waves. Moreover, the energetics and instability analyses reveal that barotropic instability dominates the energy transfer from background flow to eddies in the Kuroshio intrusion region, which energizes the surface perturbations most intensively for the looping path, followed by the leaking and leaping paths. The characteristic scales of the most unstable mode estimated by the reduced-gravity model are analogous to the observations and account for the rapid growth of surface perturbations in the Kuroshio intrusion region.

KEYWORDS: Abyssal circulation; Boundary currents; Instability

1. Introduction

The western boundary current intrusion into the marginal sea significantly contributes to the redistribution and dissipation of global oceanic energy (e.g., Ferrari and Wunsch 2009). For example, the Loop Current substantially modulates the dynamic and thermodynamic states in both the upper and deep layers of the Gulf of Mexico (Hurlburt and Thompson 1980; Hamilton 1990, 2007, 2009; Oey 1996; Oey and Lee 2002; Xu et al. 2013; Weisberg and Liu 2017; Tenreiro et al. 2018; Zhu and Liang 2020). Here, we focus on the interactions between the South China Sea (SCS) and Kuroshio intrusion, which bridge the energy and mass exchange between the SCS and the Pacific Ocean (Nan et al. 2015). Recently, a numerical study by Quan et al. (2021a) revealed that the Kuroshio intrusion and its related eddies serve as important energy sources for topographic Rossby waves (TRWs) in the northern SCS (NSCS), which dominate the intraseasonal variability of deep flow over continental slopes. This study further investigates the effect of the temporally varying Kuroshio intrusion pathway on relevant processes based on observational and theoretical analyses.

The SCS is the largest marginal sea in the northwestern Pacific Ocean, with Kuroshio intrusion through the Luzon Strait (LS) in the north (Fig. 1). Bringing in enormous mass and energy, the Kuroshio intrusion greatly constrains both the upper- and deep-layer dynamics of the NSCS (Hu et al. 2000; Qu 2000; Xue et al. 2004; Chen et al. 2011; Xu and Oey 2015; Gan et al. 2016; Zhu et al. 2017; Shu et al. 2018; Wang et al. 2021; Zheng et al. 2021). Distinct from the highly inertial Loop Current intruding into the Gulf of Mexico, the Kuroshio intrusion into the NSCS is seasonally dependent on three typical pathways, namely, the looping, leaking, and leaping paths, as shown in Fig. 1 (Nan et al. 2011a). This type of seasonality is closely connected with the rapid growth of the surface eddy kinetic energy (SEKE) in the Kuroshio intrusion region, especially in winter, which contributes greatly to the intraseasonal variability in the upper NSCS (Wang et al. 2020a,b). In this study, we demonstrate that the variable Kuroshio intrusion is also responsible for intraseasonal variability in the abyssal NSCS.

In a marginal sea with a western boundary current intrusion, deep-flow variability has often been linked to the surface eddies which are energized through baroclinic transfer (BC)

Corresponding authors: Qi Quan, qquan@sklec.ecnu.edu.cn; Ya Ping Wang, ypwang@nju.edu.cn

DOI: 10.1175/JPO-D-24-0087.1

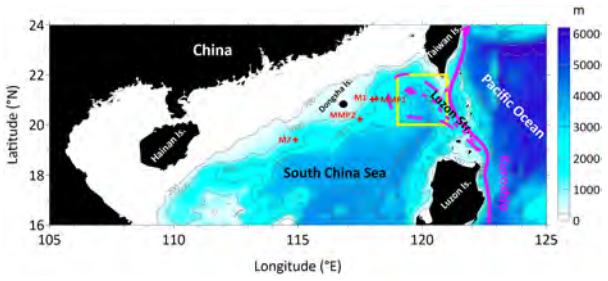

FIG. 1. Map of the NSCS. Contours are isobaths (m). Red crosses denote the mooring sites. The magenta solid, long-dashed, and short-dashed streamlines represent the leaping, looping, and leaking pathways of the Kuroshio intrusion, respectively. The yellow rectangle denotes the region which is used to compute the KSI (Huang et al. 2016).

from the background flow (e.g., Oey 2008; Donohue et al. 2016; Hamilton et al. 2019). Nevertheless, how these surface signals are transmitted to the deep had not been well demonstrated. The recent studies indicate that BC is effectively suppressed over sloping or rough topography; hence, barotropic transfer (BT) dominates the generation of eddies (LaCasce et al. 2019; Palóczy and LaCasce 2022), which has been revealed in the Gulf of Mexico by numerical models (e.g., Maslo et al. 2020; Yang et al. 2020). Furthermore, according to the theoretical and numerical studies (Tailleux and McWilliams 2001; Aoki et al. 2009; Wang and Stewart 2018; LaCasce and Groeskamp 2020; Yassin and Griffies 2022), the quasigeostrophic (QG) motions over sloping or rough topography tend to be compressed toward the surface, with the speed decaying downward to nearly zero at the bottom. This is called the surface mode, which has been proven by observations from global oceans (e.g., Wunsch 1997; de La Lama et al. 2016; Ni et al. 2023). As the surface-intensified QG motions are shielded from bottom friction, the BT-supplied eddy energy must be passed to the topographic waves for dissipation (LaCasce 2017). In this study, we first provide the observational evidence for the relevant dynamic processes in the NSCS (as far as we know).

The remainder of this paper is organized as follows: The data and methods are described in section 2. Section 3 presents the Kuroshio intrusion pathway and the associated SEKE, the resultant causality with intraseasonal variability in deep flow, and the underlying dynamics illustrated by a Kuroshio Loop Current eddy shedding (KLCES) event. The mechanism by which the high SEKE in the Kuroshio intrusion region is supplied is discussed in section 4. Finally, a summary is provided in section 5.

2. Data and methods

a. Data

Four moorings are deployed in the NSCS to reveal the dynamic connection between the deep flow and the Kuroshio intrusion (Table 1). The moorings at MMP1 and MMP2 are equipped with the McLane moored profiler (MMP), Sea Bird Equipment-37 (SBE-37) CTD, and SeaGuard RCM, whereas those at M1 and M2 are equipped with the acoustic Doppler current profiler (ADCP), SBE-37 CTD, and SeaGuard RCM. The measurement period is different for each site, spanning from May 2019 to September 2020. As we focus on intraseasonal variability, the data are filtered using a 3-day low pass to exclude the effects of high-frequency oscillations.

To identify the Kuroshio intrusion pathway and calculate SEKE in the NSCS, the daily merged absolute dynamic topography (ADT), sea level anomaly (SLA), and surface geostrophic velocity for 30 years (1993–2022) from the Copernicus Marine Environment Monitoring Service with a horizontal resolution of 1/4° are utilized. In addition, the monthly salinity from *World Ocean Atlas 2023* (*WOA23*) with a resolution of 1/4° is adopted, and ETOPO1 with a resolution of 1/60° from the National Geophysical Data Centre is used to obtain the topography.

b. Information flow–based causality analysis

To investigate the linkage between the Kuroshio intrusion and deep flow in the NSCS, we employ the causality analysis based on information flow (IF; Liang and Kleeman 2005), which has been successfully used in oceanic studies, such as the linkage between the Arctic sea ice and its potential drivers

TABLE 1. Moorings deployed in this study.

Mooring	Location	Water depth (m)	Measurement period	Instrument	Measurement range (m)
MMP1	21.04°N, 118.16°E	2050	27 Sep 2019–21 Sep 2020	MMP CTD RCM	0–2000
M1	21.02°N, 117.99°E	1600	28 Sep 2019–21 Sep 2020	Upward 75-kHz ADCP Downward 150-kHz ADCP CTD RCM	0–1500
MMP2	20.23°N, 117.49°E	2050	29 Sep 2019–23 Sep 2020	MMP CTD RCM	0–2000
M2	19.40°N, 114.90°E	1543	13 May 2019–16 Sep 2020	Upward 300-kHz ADCP CTD RCM	0–1480

(Docquier et al. 2022), the remote connection between the Kuroshio intrusion into the NSCS and the downstream intrusion into the East China Sea (Zhao et al. 2023), and the relation between the Loop Current penetration and the inflow/outflow in the Gulf of Mexico (Yang et al. 2023).

Consider a 2D stochastic system with the state variables $\mathbf{X} = (X_1, X_2) \in \mathbb{R}^2$. Let ρ be the joint probability density. Then, we have the marginal probability density of X_1, $\rho_1 = \int_{\mathbb{R}} \rho dX_2$, and the marginal entropy of X_1, $H_1 = -\int_{\mathbb{R}} \rho_1 \log \rho_1 dX_1$. The time rate of change of H_1, $dH_1/dt = dH_1^*/dt + dH_1^{\text{noise}}/dt + T_{2\to1}$, is owing to two different mechanisms, one due to X_1 itself with $dH_1^*/dt = E(\partial F_1/\partial X_1)$ (dH_1^{noise}/dt) having no (having) stochasticity and another due to the very IF from X_2 to X_1, which can be written as

$$T_{2\to1} = -E\left[\frac{1}{\rho_1}\frac{\partial(F_1\rho_1)}{\partial X_1}\right] + \frac{1}{2}E\left[\frac{1}{\rho_1}\frac{\partial^2(b_{11}^2 + b_{12}^2)\rho_1}{\partial X_1^2}\right], \tag{1}$$

where F_1 is the drift coefficient, E is the mathematical expectation, and b_{ij} is the diffusion coefficient. In the case when only two time series are available, Eq. (1) can be statistically estimated under the linear assumption (Liang 2014):

$$\hat{T}_{2\to1} = \frac{C_{11}C_{21}C_{2,d1} - C_{12}^2C_{1,d1}}{C_{11}^2C_{22} - C_{11}C_{12}^2}, \tag{2}$$

where C_{ij} is the sample covariance between X_i and X_j ($i, j = 1, 2$), $C_{i,dj}$ is the covariance between X_i and $\dot{X}_j$, and $\dot{X}_j$ is the difference approximation of dX_j/dt using the Euler forward scheme. Note that Eq. (2) is also valid in highly nonlinear systems (Liang 2014). The IF satisfies the principle of nil causality (Liang 2016a); that is, if the evolution of X_1 is independent of X_2, then $T_{2\to1} = 0$; otherwise, $T_{2\to1} \neq 0$. Moreover, the IF is asymmetric between X_1 and X_2, that is, $T_{2\to1} \neq T_{1\to2}$.

To quantify the relative importance of the causalities among different factors, Eq. (1) is normalized as follows:

$$\tau_{2\to1} = \frac{T_{2\to1}}{\left|\frac{dH_1}{dt}\right|}. \tag{3}$$

If $\tau_{2\to1} = 1$, the evolution of H_1 is completely attributed to the IF from X_2; if $\tau_{2\to1} = 0$, X_2 is not causal to X_1. A detailed derivation can be found in Liang (2008, 2014, 2015, 2016a) and references therein. Note that all the IFs shown in this study are normalized and pass the statistical significance test at the 99% confidence level.

c. Barotropic instability analysis

Because the QG motions over the continental slope of the NSCS have been suggested to be surface intensified (Quan et al. 2023) and the mean flow in the Kuroshio intrusion region is dominated by its zonal component (see section 4) and also the BT dominates the upper-layer energy transfer between the mean flow and eddies in this region (Yang et al. 2013; Zhang et al. 2017; also see appendix), we use a 1.5-layer reduced-gravity model (a crude representation of surface mode; LaCasce 2017) with a meridionally sheared mean flow $U(y)$ to investigate the characteristic scales of the most unstable waves in the Kuroshio intrusion region for different pathways. According to Qiu and Chen (2004), the linearized equations for the perturbation velocity $\mathbf{v}$ and thickness h in the model can be written as

$$\frac{\partial \mathbf{v}}{\partial t} + U\frac{\partial \mathbf{v}}{\partial x} + v\frac{\partial U}{\partial y}\mathbf{i} + f\mathbf{k} \times \mathbf{v} = -g'\nabla h \quad \text{and} \tag{4}$$

$$\frac{\partial h}{\partial t} + U\frac{\partial h}{\partial x} + v\frac{\partial H}{\partial y} + H\nabla \cdot \mathbf{v} = 0, \tag{5}$$

where f is the Coriolis parameter, g' is the reduced gravity, and $H(y)$ is the mean upper-layer thickness in the geostrophic balance with U through $fU = -g'H_y$. Equations (4) and (5) can be combined to obtain the potential vorticity (PV) equation as follows:

$$\left(\frac{\partial}{\partial t} + U\frac{\partial}{\partial x}\right)q + v\frac{\partial Q}{\partial y} = 0, \tag{6}$$

where $Q = (f - U_y)/H$ and $q = (1/H)[\partial v/\partial x - \partial u/\partial y] - (h/H)Q$ denote the mean and perturbation PVs, respectively. Assuming that the perturbation motions are quasigeostrophic (i.e., $f\mathbf{k} \times \mathbf{v} = -g'\nabla h$), we can pursue the normal-mode solution $h = \text{Re}[A \exp ik(x - ct)]$ of Eq. (6) and have

$$\frac{d^2}{dy^2}A - (k^2 + R_d^{-2})A + \frac{\beta - U_{yy} + UR_d^{-2}}{U - c}A = 0, \tag{7}$$

where A is the amplitude, k is the zonal wavenumber, $c = c_r + ic_i$ is the phase speed, $\beta = \partial f/\partial y$ is the meridional gradient of the Coriolis parameter, and $R_d = \sqrt{g'H}/f$ is the internal Rossby deformation radius.

Equation (7) is the eigenvalue problem for the BT analysis of the meridionally sheared flow $U(y)$ if c is regarded as the eigenvalue. Here, $g' = 0.03$ m s^{-2} and $H = 200$ m are used according to Wang et al. (2008). Because full-depth observations for the current in the Kuroshio intrusion region are unavailable, the satellite-observed surface geostrophic velocities averaged between 118° and 120°E along the section from 20° to 22.5°N for different pathways are used to obtain $U(y)$ and U_{yy} (see section 4).

3. Results

a. Kuroshio intrusion pathway and SEKE

There exist many indices that were employed to depict the state of the Kuroshio intrusion into the NSCS (e.g., Wu 2013; Sun et al. 2021; Zhao et al. 2023). However, most of them can only distinguish the patterns in which the Kuroshio penetrated or not, but the looping and leaking paths cannot be further separated. Moreover, the thresholds of these indices were not quantified and hence difficult to use for the present pursuit. To identify the three types of Kuroshio intrusion pathway in the NSCS, we use satellite data to calculate the Kuroshio-SCS index (KSI) proposed by Nan et al. (2011a), namely, the area-integrated relative vorticity in the yellow rectangle in Fig. 1, as follows:

$$\text{KSI} = \iint [-(g/f)\nabla^2\eta]dS, \tag{8}$$

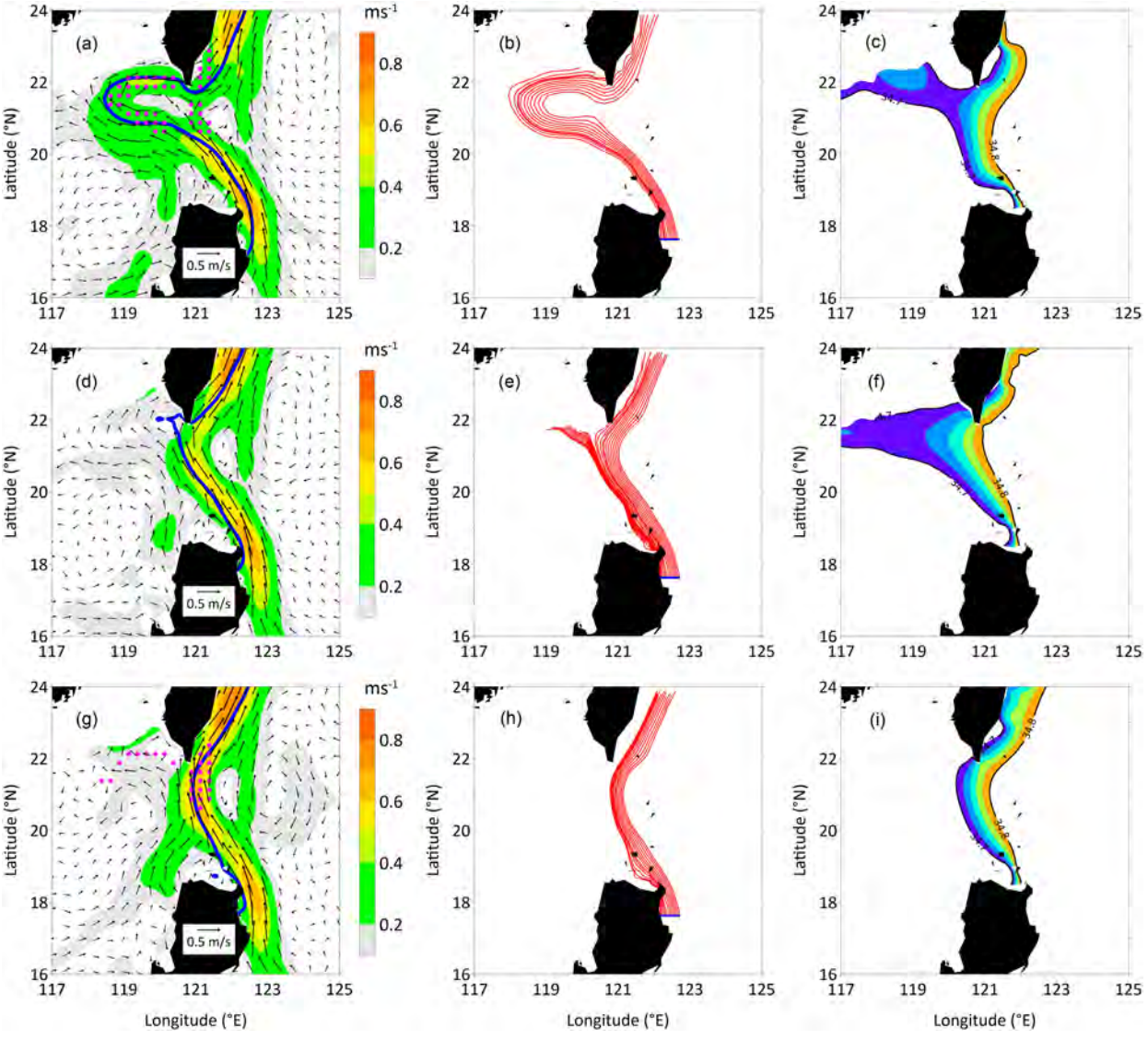

FIG. 2. (a) Satellite-observed mean surface geostrophic currents (m s^{-1}) associated with the looping pathway of the Kuroshio intrusion from 1993 to 2022. Blue solid lines denote the ADT contour of 115 cm. Magenta dots represent the regions where the currents are substantially distinct from the climatology with the 95% confidence level. Note that regions shallower than 200 m are masked. (b) Trajectories of the particles released at the section (122.125°–122.625°E, 17.625°N; blue solid line) east of the Luzon Island, which are based on the current field in (a) and traced for 30 days. (c) Maximum salinity at 150 m in February from the *WOA23*, in which only the isohalines between 34.7 and 34.8 with an interval of 0.02 are shown. (d)–(f),(g)–(i) As in (a)–(c), but for the leaking (with the representative salinity in October) and leaping (with the representative salinity in August) pathways of the Kuroshio intrusion, respectively.

where η is the ADT. Note that the integration region (119°–121°E, 20°–22°N) used here is smaller than that in Nan et al. (2011a) to avoid the misjudgment owing to the offset between the positive and negative vorticities (Huang et al. 2016). The results are normalized by subtracting the mean value and dividing by the standard deviation. According to Nan et al. (2011a), the looping (leaping) path corresponds to a dimensionless KSI lower (higher) than −1 (+1), and the leaking path occupies a KSI falling in between. Following Nan (2012), we also add the satellite-observed surface Luzon Strait transport (SLST) through 121°E as an additional constraint to connect the KSI with water exchange, i.e., leaping path for an eastward SLST and looping path for a westward SLST. This constraint can improve the significance of the results and their consistency with the previous studies.

The left panel in Fig. 2 shows the mean surface geostrophic current associated with the three pathways of the Kuroshio intrusion in the NSCS from 1993 to 2022. Considering the possible indistinguishability in the flow field, e.g., the branch leaking from the Kuroshio mainstream that tends to merge within the cyclonic gyre in the interior NSCS (Fig. 2d), we perform the Lagrangian tracing based on the current [Tracing

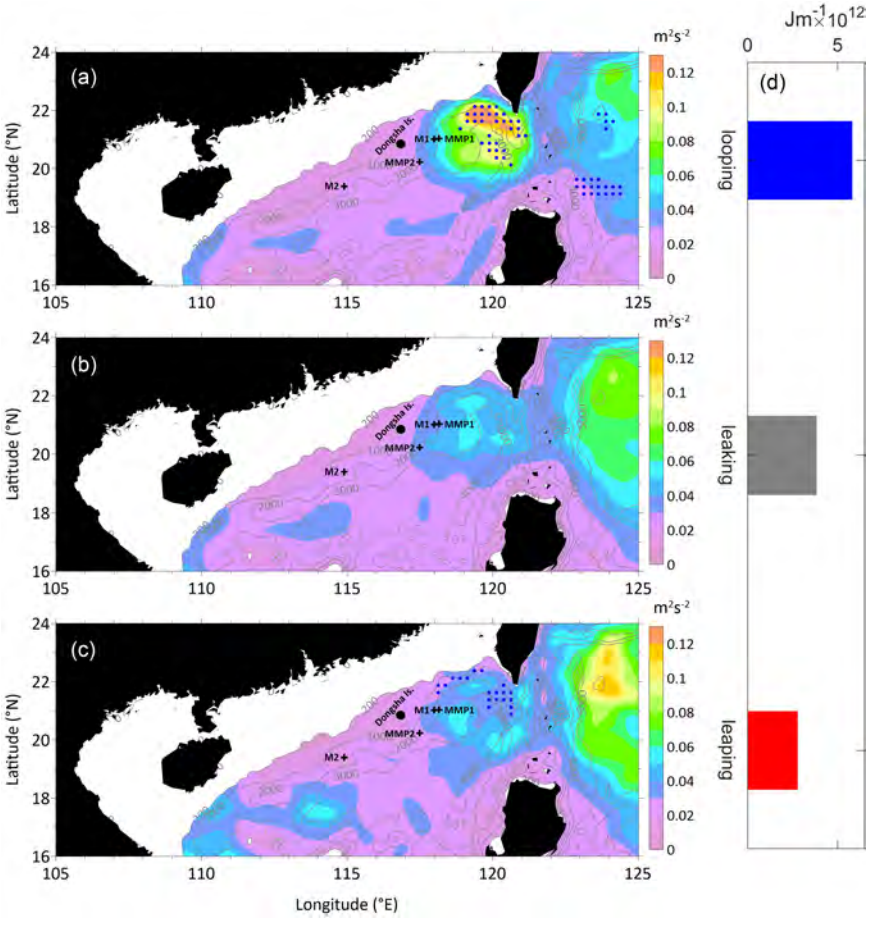

FIG. 3. (a) Mean SEKE ($m^2\ s^{-2}$) associated with the looping pathway of the Kuroshio intrusion. Contours denote the isobaths. Blue dots represent the regions where the SEKE deviates substantially from the climatology with the 95% confidence level. Note that regions shallower than 200 m are masked. (b),(c) As in (a), but for the leaking and leaping paths, respectively. (d) Area-integrated SEKE ($J\ m^{-1}$) in the Kuroshio intrusion region (yellow rectangle in Fig. 1) for the three paths. Note that the results are multiplied by the reference density of 1025 kg m^{-3}.

the Water Masses of the North Atlantic and the Mediterranean (TRACMASS); Jönsson et al. 2015] and show trajectories of the particles, which are released at the section (122.125°–122.625°E, 17.625°N) east of the Luzon Island and traced for 30 days, to better demonstrate the pathways from the perspective of mass transport (middle panel in Fig. 2). Moreover, we also display the observed maximum salinity at 150 m from the *WOA23* to support the results of particle tracing (right panel in Fig. 2). Note that the representative months for different pathways are selected according to the maximum occurrence probabilities shown in Figs. 4b–d.

For the looping path (Figs. 2a–c), the Kuroshio enters the NSCS in the middle of the LS and leaves in the north, forming an anticyclonic loop with the salinity higher than the surroundings. For the leaking path (Figs. 2d–f), the Kuroshio veers northeastward in the northern half of the LS, with a branch intruding into the NSCS from the southwest of Taiwan (see the particle trajectories and the salty water extending northwestward). For the leaping path (Figs. 2g–i), the Kuroshio barely enters the NSCS and strides over the LS. The crucial dynamics for the multipath variability of the Kuroshio intrusion is attributed to the competition between beta effect and inertia effect (which is predominantly determined by the flow strength over the gap), the former favoring a penetrating state and the latter favoring a leaping state (Sheremet 2001). Therefore, the fundamental difference between the leaking and leaping paths appears at the south and southwest of Taiwan, where the Kuroshio is intensified for the leaping path and hence has no branch intruding into the NSCS. In addition, previous studies have suggested that the westerly wind anomaly in the tropical Pacific (Wang et al. 2006), the negative wind stress curl off southwest Taiwan (Wu and Hsin 2012), the impingement of cyclonic eddies from the Pacific (Yuan and Wang 2011), the double-gyre circulation in the SCS (Mei et al. 2023), and even the downstream intrusion into the East China Sea (Zhao et al. 2023) are also responsible for the path transition from the leaping to the penetrating states. Such Kuroshio path variability has been thought to dominate eddy generation in the relevant region

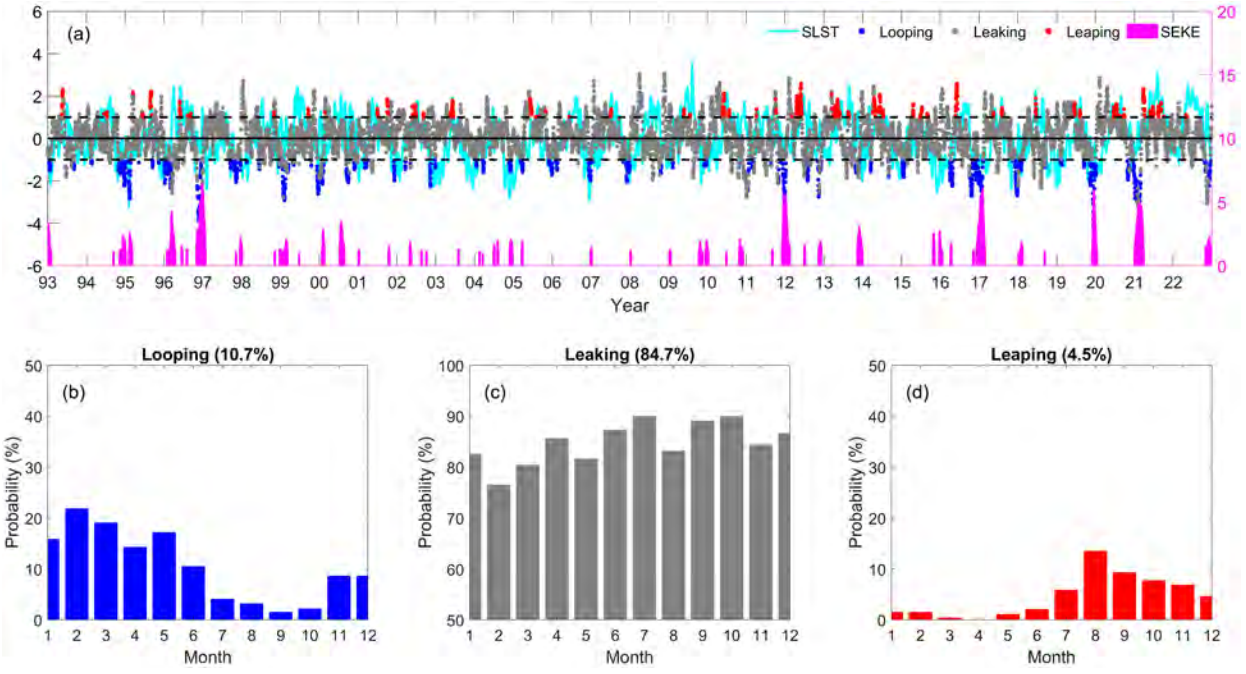

FIG. 4. (a) Time series of the daily KSI, SLST, and SEKE integrated within the yellow rectangle in Fig. 1. Note that the results are normalized by subtracting the mean value and dividing by the standard deviation. The KSI identifies the type of the Kuroshio intrusion pathway, with the blue, gray, and red dots denoting the looping, leaking, and leaping paths, respectively. The black dashed lines represent the absolute values equal to 1. Note that only the SEKE substantially higher than the climatological mean with the 95% confidence level is shown. (b)–(d) Monthly occurrence probability for the looping, leaking, and leaping path, respectively.

(Nan et al. 2011b), which inspires the present study and will be further demonstrated below.

To investigate the influence of the variable Kuroshio intrusion pathway on the upper NSCS, we calculate the SEKE and show the results in Fig. 3. Collocated with the high eddy activity region (Chen et al. 2011; He et al. 2018), the Kuroshio intrusion region occupies the highest SEKE in the NSCS, wherein the energy is strongest for the looping path, followed by the leaking and leaping paths. The pattern for the leaping path is similar to that for the leaking path but weaker off the southwest Taiwan. These results suggest that the background flow in the Kuroshio intrusion region is highly unstable, particularly for the looping path, which contributes greatly to the variation of SEKE in this area.

To further explore the evolution of the Kuroshio intrusion pathway and its related effect, time series of the daily KSI, SLST, and area-integrated SEKE in the Kuroshio intrusion region are shown in Fig. 4. In the 30-yr observation period, the occurrence probabilities for the three pathways of the Kuroshio intrusion are 10.7% (looping; 1177 days), 84.7% (leaking; 9286 days), and 4.6% (leaping; 494 days), respectively. It suggests that the leaking path is most frequent and hence can be regarded as the climatology to some extent because their difference is insignificant under the *t* test with the 95% confidence level (not shown), whereas the looping (leaping) path is transient and prefers to occur in winter (summer). The occurrence probabilities of the looping and leaping paths are slightly lower than those reported by Nan et al. (2011a) because of the additional constraint from the SLST, which regards the events (mostly in winter) with a KSI lower (higher) than −1 (+1) but a westward (eastward) SLST as the leaking rather than the leaping (looping) path. Considering the good correlation (~0.6) between the KSI and SLST, this constraint can effectively improve the significance of the identification to the 95% confidence level and also make the results more consistent with the previous studies. For example, the Kuroshio has been suggested to meander anticyclonically to a significant extent into the NSCS in winter but tend to stride over the LS in summer (e.g., Yuan et al. 2006; Wu et al. 2017). This contrasting winter–summer behavior agrees well with the occurrence probabilities of the looping and leaping paths shown here. In addition, the SEKE in the Kuroshio intrusion region appears to peak in winter (Wang et al. 2020a,b), which is also consistent with the occurrence of the looping path and the high SEKE events shown in Figs. 3a and 4a, 4b. These results suggest significant seasonality for the variable Kuroshio intrusion pathway in the NSCS, which can substantially modulate the upper-layer dynamics west of the LS.

b. Intraseasonal variability in deep flow

Consistent with previous observations in the NSCS (Wang et al. 2019; Wang et al. 2021; Zheng et al. 2021; Shu et al. 2022), energetic intraseasonal variability in the deep flow, with the amplitudes (0.03–0.07 m s^{-1}) comparable to the mean flow and significant spectral peaks at 7–15 days, is also revealed by our moorings (Fig. 5). These subinertial fluctuations, which

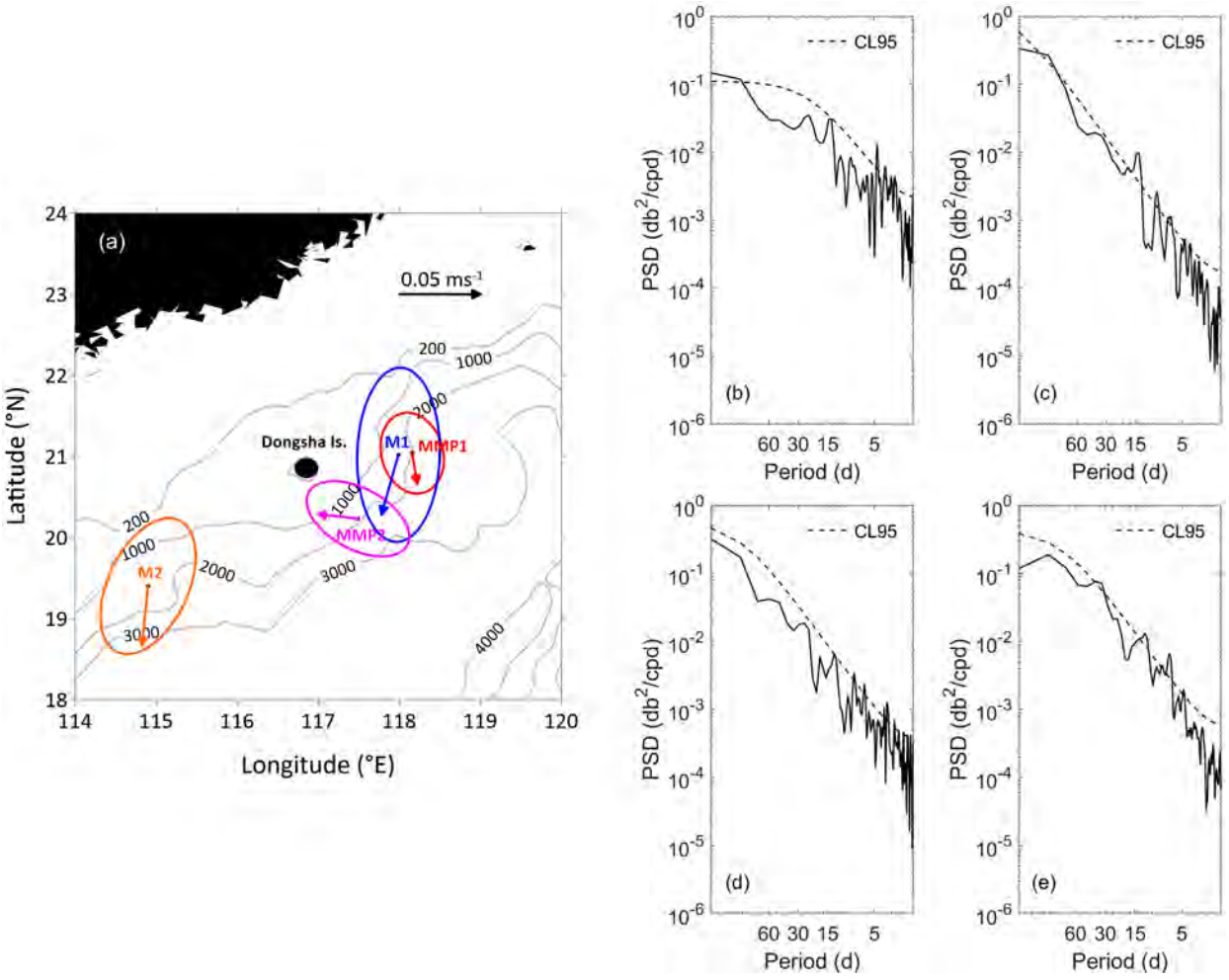

FIG. 5. (a) Mean velocity and standard deviation ellipse of the bottom flow at each site. (b)–(e) Power spectra of the BPA at MMP1, M1, MMP2, and M2, respectively. Dashed lines denote the 95% confidence level (CL95).

are attributed to TRWs (Quan et al. 2021b), account for over 40% of the total variance in the deep layer (not shown). According to the numerical study by Quan et al. (2021a), the energy source of TRWs in the abyssal NSCS can be traced back to the SEKE in the Kuroshio intrusion region. However, the westward propagation of TRWs generated east of the Dongsha Islands may be overestimated because of the over smoothed topography in the numerical model, which will be demonstrated in the following sections.

Figure 6 shows the time series of the daily SEKE integrated in the Kuroshio intrusion region from October 2019 to September 2020 and those at the mooring sites, the latter are overlapped by the concurrent bottom pressure anomaly (BPA), which is observed by CTD and obtained by subtracting the mean value in the measurement period. In general, the seasonality of SEKE at MMP1, M1, and MMP2 (Figs. 6b–d), which are close to the Kuroshio intrusion region, is similar to that shown in Fig. 6a, whereas it is slightly different at the distant M2 (Fig. 6e), with the time lags closely associated with the KLCES event (see section 3c). High coherence between the upper and deep layers occurs if the dimensionless SEKE is larger than 1, which can be attributed to the local effect through vertical pressure work (Quan et al. 2021a). Such linkage is strongest for the maximum SEKE and BPA observed within the KLCES event related to the looping path in winter (also see section 3c), while it appears to be weaker for other paths. Note that the variability in BPA does not always respond to surface perturbations, particularly at M2. According to Quan et al. (2021b), TRWs in the abyssal NSCS are energized primarily through vertical pressure work, but the waves can also be forced by BC or BT in the deep layer or propagated upstream. These local and remote effects are usually mixed and hard to be distinguished.

To determine the local and remote effects as quantitatively as possible, we employ the IF-based causality analysis described in section 2b. First, we calculate the IF from local SEKE to BPA at each site (Fig. 7a). The results indicate that IF is largest at M1, followed by MMP2 and MMP1, but is nearly zero at M2. It suggests that the deep oscillations at MMP1, M1, and MMP2 are associated with local surface

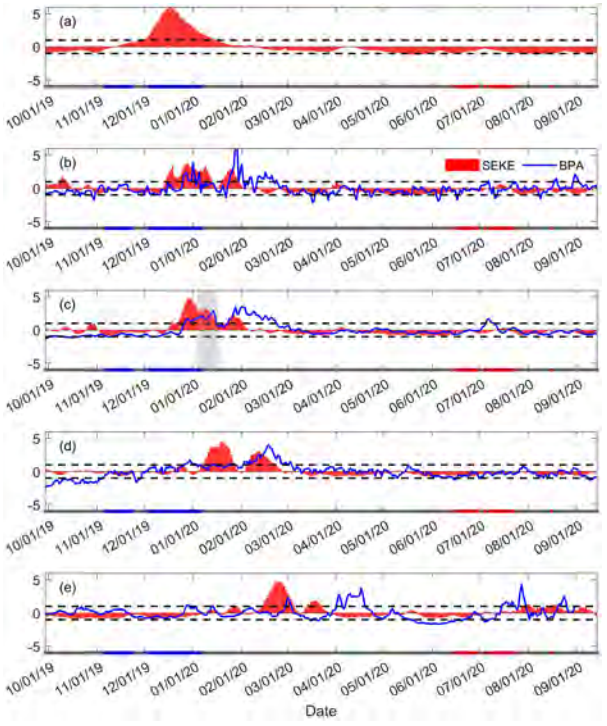

FIG. 6. (a) SEKE integrated in the Kuroshio intrusion region from October 2019 to September 2020. (b) Time series of the SEKE and 3-day low-pass-filtered BPA at MMP1. (c)–(e) As in (b), but for M1, MMP2, and M2, respectively. Note that all the results are normalized by subtracting the mean value and dividing by the standard deviation. The black dashed lines represent the absolute values equal to 1. Dates on which the looping, leaking, and leaping pathway of the Kuroshio intrusion occurred are colored in blue, gray, and red, respectively. The period when the eddy reached and passed through M1 is shaded.

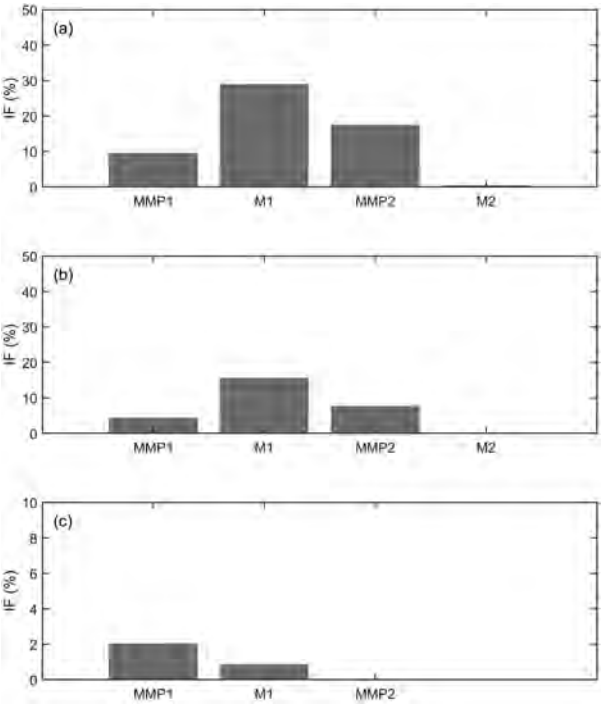

FIG. 7. (a) IFs from the local SEKE to BPA at the mooring sites. (b) As in (a), but for IFs from the area-integrated SEKE in the Kuroshio intrusion region (yellow rectangle in Fig. 1) to BPA at the mooring sites. (c) IFs from BPA at MMP1, M1, and MMP2 to that at M2, respectively.

perturbations, whereas such a causality is not significant at M2. This is consistent with the model results in Quan et al. (2021a) that the cross-layer interactions are active east of the Dongsha Islands, where the SEKE is highest in the NSCS (Fig. 3). Note that the difference between the adjacent sites MMP1 (~2050 m) and M1 (~1600 m) likely arises from the drastic change in bathymetry, which can affect the vertical coupling greatly (LaCasce 2017; Quan et al. 2023). We then calculate the IF from the SEKE integrated in the Kuroshio intrusion region to BPA at each site (Fig. 7b). The results are very similar to those in Fig. 7a, suggesting that the deep oscillations at MMP1, M1, and MMP2 (excluding M2) can also be remotely linked to surface perturbations in the Kuroshio intrusion region. Finally, we calculate the IFs from BPA at MMP1, M1, and MMP2 to that at M2 (Fig. 7c). The results show that the deep oscillations at M2 are weakly affected by the upstream. An analogous result is also obtained by the lead–lag correlation analysis (not shown). This deviates from the backward ray tracing analysis by Quan et al. (2021a), suggesting that TRWs generated east of the Dongsha Islands would dissipate rapidly and have limited influence on the downstream. The experimental and numerical results in Stewart et al. (2011) have suggested that TRWs would break if the topography varies intensively. Considering the sharp topographic variation near the Dongsha Islands (see Fig. 5a), previous numerical models with smoothed topography probably overestimated the westward propagation of TRWs in the NSCS. The generation of TRWs at M2 may be related to BC or BT in the deep layer, which remains to be addressed with additional observations in the future.

As the causalities between BPA and local-remote SEKE have been revealed, we further calculate the IFs from the area-integrated SEKE in the Kuroshio intrusion region to the SEKE at each grid in the NSCS (Fig. 8a). The significant IFs reside in the area east of the Dongsha Islands, which covers the mooring sites MMP1, M1, and MMP2. This implies that the energetic surface perturbations originating from the Kuroshio intrusion region can substantially modulate SEKE in this area, which accounts for the connection between Figs. 7a and 7b. By investigating the long-lived (>30 days) eddies generated in the Kuroshio intrusion region and their pathways in the past 30 years (Fig. 8b), we find that these eddies contributed ~1/5 of the total number in the NSCS and tended to be trapped by the continental slope during their westward migration. Most of these eddies decayed completely east of the Dongsha Islands, which is consistent with the distribution of significant IFs in Fig. 8a.

These results suggest that the high SEKE associated with the variable Kuroshio intrusion in the NSCS can energize

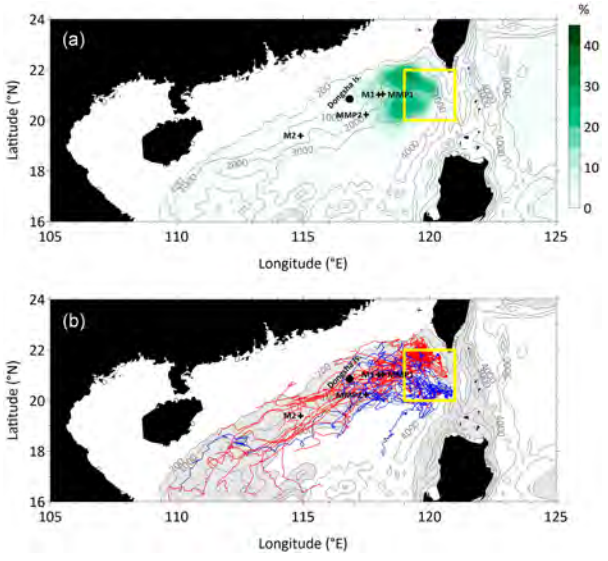

FIG. 8. (a) IFs from the area-integrated SEKE in the Kuroshio intrusion region (yellow rectangle) to the SEKE at each grid in the NSCS. (b) Pathways of anticyclonic (red) and cyclonic (blue) eddies generated in the Kuroshio intrusion region from 1993 to 2022. Note that only the eddies with a lifespan over 30 days are counted. The continental slope regions (200–3000 m) are shaded.

intraseasonal variability in the deep flow east of the Dongsha Islands. The underlying dynamics for the general situation, as well as the KLCES event, have been revealed in the model study by Quan et al. (2021a). The numerical results show a similar mechanism therein (i.e., the coupling between layers is fulfilled through vertical pressure work), besides the particularly strong vertical energy transfer for the KLCES event (consistent with the observational results shown in Fig. 6). Considering that an intensive KLCES event was captured by our moorings, the relevant mechanism will be further verified by observations in the following section.

c. *KLCES event*

As shown in Figs. 3a, 4a, and 4b, the significantly enhanced SEKE west of the LS in winter has been suggested to be closely associated with the KLCES events (Nan et al. 2011b; Zhang et al. 2017). Different from most of the eddies decaying east of the Dongsha Islands, these shedding anticyclonic eddies can migrate westward for a very long distance and even cross the entire NSCS (Fig. 8b). For example, the KLCES event occurred in late December 2019 and lasted for approximately 3 months (Fig. 9). This is one of the most intensive KLCES events in the past 10 years (Liu et al. 2023), which contributes greatly to the maximum SEKE and BPA at the mooring sites during its westward migration (see Fig. 6). Taking this event as a representative example, we will demonstrate the underlying dynamics of the vertical coupling between the surface perturbation and deep flow described in section 1.

To illustrate the modal structure of the surface perturbation, we first calculate the principal EOFs of the observed velocity profiles during the eddy transit at M1 (note that the full-depth observation for the current is available only at this site) and impose the analytical solution of the surface mode with a sloping bottom for comparison:

$$\phi(z) = \phi_0 e^{z/d}[Y_0(\gamma)J_1(\gamma e^{z/d}) - J_0(\gamma)Y_1(\gamma e^{z/d})], \tag{9}$$

where $\gamma = N_0 d\lambda/f$; $\lambda^2 = -[k^2 + l^2 + \beta/(k\omega)]$; ω is the frequency; d is the e-folding scale of the buoyancy frequency $N = N_0 e^{z/d}$; and J_n and Y_n are the Bessel functions with n being the order (LaCasce 2017). Here, we use the typical parameters $N_0 = 2 \times 10^{-2}$ s^{-1} and $d = 300$ m in the NSCS (Wang et al. 2019). Figure 10 shows that the primary modal structures of the observed velocity profiles (accounting for over 90% of the total variance) are consistent with the theoretical estimation, except for the zonal component near the bottom. Note that the numerical solution with an observational profile of N can be more precise. Unfortunately, full-depth CTD data are unavailable. These results suggest that the energy was compressed toward the surface when the eddy passed over the continental slope. Further details regarding the surface modes observed in the NSCS can be found in Quan et al. (2023).

According to LaCasce (2017), surface-intensified eddy energy must be passed to topographic waves to be dissipated. Based on this, we investigate the cross-layer energy transfer associated with interface motions, namely, the vertical pressure work:

$$\Delta_z Q_P = -\frac{\partial}{\partial z}\left(\frac{1}{\rho_0} pw\right), \tag{10}$$

where p is the pressure, w is the vertical velocity, and $\rho_0 = 1025$ kg m^{-3} is the reference density of seawater. Considering that the vertical velocity and the horizontal mass flux are incalculable, Eq. (10) is simplified under the assumptions $w \approx -\rho_t/\rho_z$ and $\partial w/\partial z \approx 0$ as follows:

$$\Delta_z Q_P = -\frac{\rho_t p - \rho_0 p_z(\rho_t/\rho_z)}{\rho_0^2}, \tag{11}$$

where ρ_t is the time rate of change of potential density, ρ_z is the vertical gradient of potential density, and p_z is the vertical gradient of pressure. For comparison between layers, the time series of the potential density, pressure, vertical pressure work (computed at 250 and 1450 m), and kinetic energy in the upper (200 and 300 m) and deep (1400 and 1500 m) layers for the eddy transit at M1 are normalized, as shown in Fig. 11. When the eddy reached and passed through this site from 4 to 17 January 2020 (shaded), the interfaces were distorted, and the variations in potential density and pressure led to positive (negative) vertical pressure work in the deep (upper) layer, indicating a downward energy transfer. This process substantially energized (dissipated) the abyssal TRWs (surface eddy), which is also reflected in the weakened SEKE and enhanced BPA, as shown in Fig. 6c (shaded). Subsequently, the interfaces

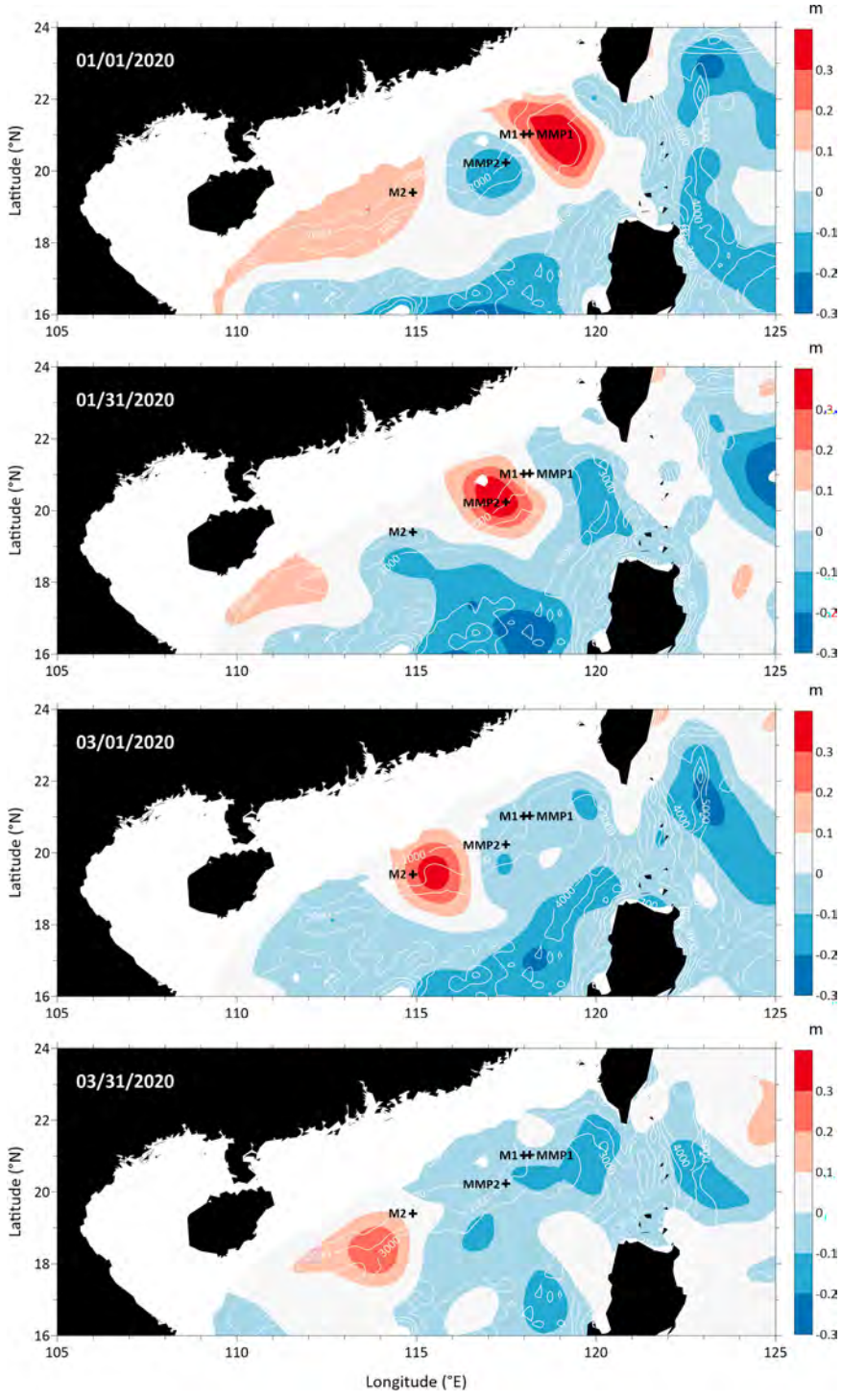

FIG. 9. Satellite-observed SLA (m) during a KLCES event from 1 Jan to 31 Mar 2020 with a 30-day interval. White contours denote the isobaths. Note that regions shallower than 200 m are masked.

oscillated for days until the energy was dissipated (not shown). These observations verify the relevant mechanism revealed by the numerical model in the NSCS (Quan et al. 2021a,b, 2022) and agree with the studies on global oceans (e.g., Wunsch and Ferrari 2004; Zhai and Marshall 2013; Chen et al. 2014; Maslo et al. 2020; Yang et al. 2020), which suggests that vertical pressure work plays a critical role in energy exchange across layers.

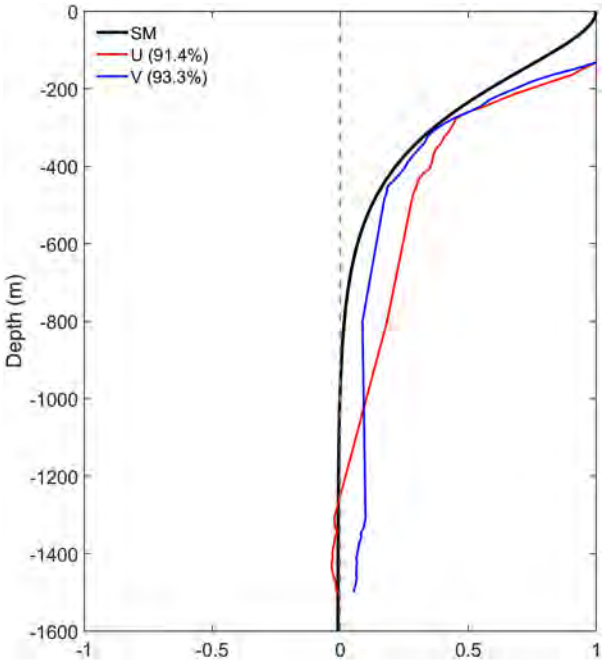

FIG. 10. Principal EOFs of zonal (red) and meridional (blue) velocity components at M1 from 1 to 30 Jan 2020, in comparison with the analytical solution for surface mode (black) using an exponential profile of buoyancy frequency. Note that results are divided by the maximum of respective profiles for normalization.

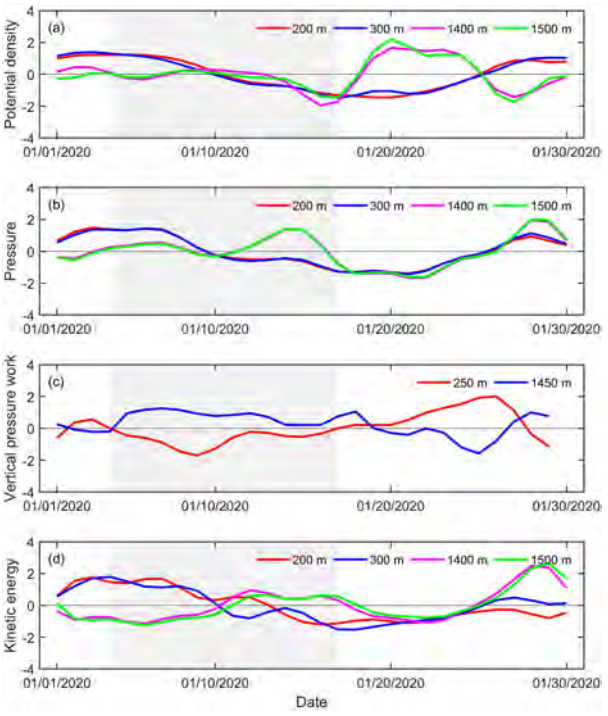

FIG. 11. Time series of the 3-day low-pass-filtered (a) potential density, (b) pressure, (c) vertical pressure work (computed at 250 and 1450 m), and (d) kinetic energy in the upper (200 and 300 m) and deep (1400 and 1500 m) layers for the eddy transit at M1. The period during 4–17 Jan 2020 is shaded to highlight the process of downward energy transfer. Note that results are normalized by subtracting the mean value and dividing by the standard deviation.

4. Discussion

We have demonstrated that the variable Kuroshio intrusion is causal to the high SEKE east of the Dongsha Islands, particularly for the looping path in winter. These intensive surface perturbations are compressed in the upper layer, and their energy is partially transferred downward through vertical pressure work to force the abyssal TRWs. In this section, how the surface perturbations gain energy from the background flow in the Kuroshio intrusion region is discussed.

Following Liang and Robinson (2007), we first calculate the BT and BC by using a numerical model to compare their relative importance in the energy transfer between the background flow and eddies in the Kuroshio intrusion region:

$$\mathrm{BT} = \frac{1}{2}\rho_0\{[\overline{u}\nabla\cdot\overline{(u'\mathbf{v}')} + \overline{v}\nabla\cdot\overline{(v'\mathbf{v}')}] - [\overline{u'\mathbf{v}'}\cdot\nabla\overline{u} + \overline{v'\mathbf{v}'}\cdot\nabla\overline{v}]\}, \tag{12}$$

$$\mathrm{BC} = \frac{c}{2}\rho_0[\overline{(\rho'\mathbf{v}')}\cdot\nabla\overline{\rho} - \overline{\rho}\nabla\cdot\overline{(\rho'\mathbf{v}')}],\ c = g^2/(\rho_0 N)^2, \tag{13}$$

where the overbars and primes denote the temporal mean (1 month) and anomalies from the mean, respectively. Note that both the velocity and density act as a function of depth. Consistent with the previous studies (Yang et al. 2013; Zhang et al. 2017), the results suggest a dominant role for BT in the relevant process (see appendix). Based on this, we further utilize the observed surface geostrophic velocity to calculate BT and the area-integrated results in the Kuroshio intrusion region are shown in Fig. 12. Similar to the modeled results, the observational BT largely accounts for the variation of SEKE in this region (with a correlation coefficient of ~0.6 at the 95% confidence level). This again suggests that background flow over sloping topography tends to be barotropically unstable (LaCasce et al. 2019; Palóczy and LaCasce 2022).

To further compare the pattern and intensity of BT among the three pathways of the Kuroshio intrusion, we show the relevant maps in Fig. 13 (note that only the positive values are exhibited to indicate the energy transfer from background flow to eddies). Consistent with the results shown in Fig. 3, the highest BT also occurs in the Kuroshio intrusion region, wherein the energy transfer is strongest for the looping path, followed by the leaking and leaping paths. The pattern for the leaping path is similar to that for the leaking path but weaker off the southwest Taiwan. These results demonstrate again that the background flow in the Kuroshio intrusion region tends to be unstable, particularly for the looping path, which results in significant seasonality of SEKE in this region. More details about the eddy generation owing to change of the Kuroshio intrusion path can be referred to Nan et al. (2011b).

Finally, we investigate the characteristic scales of the most unstable mode of background flow in the Kuroshio intrusion region for each pathway by using the reduced-gravity model

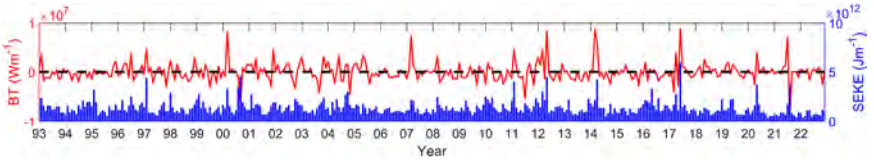

FIG. 12. Area-integrated BT (W m^{-1}; red) and SEKE (J m^{-1}; blue) in the Kuroshio intrusion region (yellow rectangle in Fig. 1) from 1993 to 2022. The black dashed line denotes the zero value for BT. Note that positive values for BT indicate the energy transfer from the background flow to eddies, and vice versa.

described in section 2c (note that the relevant temporal scale reflects the growth time of perturbation rather than the duration of pathway). Taking the dominant zonal component U as the simplification of the background flow (Figs. 14a–c), we solve Eq. (7) numerically and acquire the eigenvalue c with a nonzero imaginary part, which represents a growing unstable wave:

$$h = \mathrm{Re}[A(y)e^{kc_i t}e^{i(kx-c_r t)}], \tag{14}$$

where kc_i denotes the growth rate. The results for the maximum kc_i are presented as a function of the zonal wavenumber k in Fig. 14d. Consistent with the intensities of BT shown in Fig. 13, the unstable wave grows fastest for the looping path, with the characteristic scales of 70.0 km and 15.6 days. The

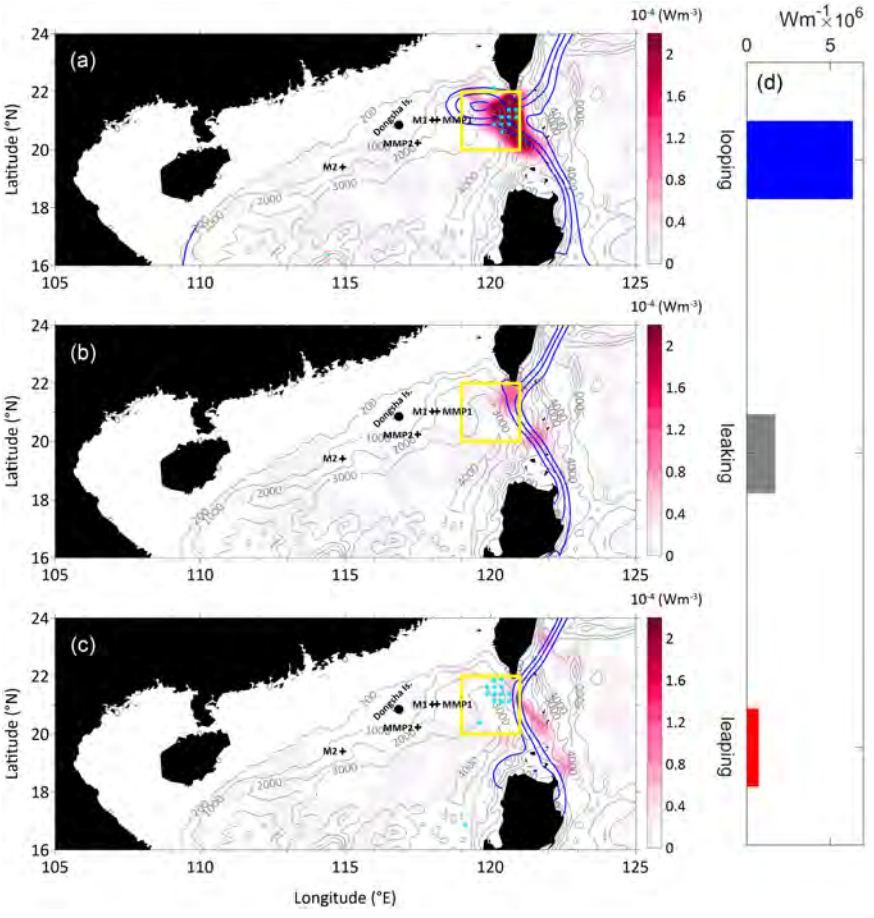

FIG. 13. (a) Surface BT (W m^{-3}) associated with the looping pathway of the Kuroshio intrusion. Only the positive values are shown to suggest the energy transfer from background flow to eddies. The blue contours denote the ADT of 115–125 cm with an interval of 5 cm. The gray contours are the isobaths. The yellow rectangle denotes the Kuroshio intrusion region. Cyan dots represent the regions where the results are substantially distinct from the climatology with the 95% confidence level. Note that regions shallower than 200 m are masked. (b),(c) As in (a), but for the leaking and leaping paths, respectively. (d) Area-integrated surface BT in the Kuroshio intrusion region for the three paths. Note that only the positive values are used for calculation.

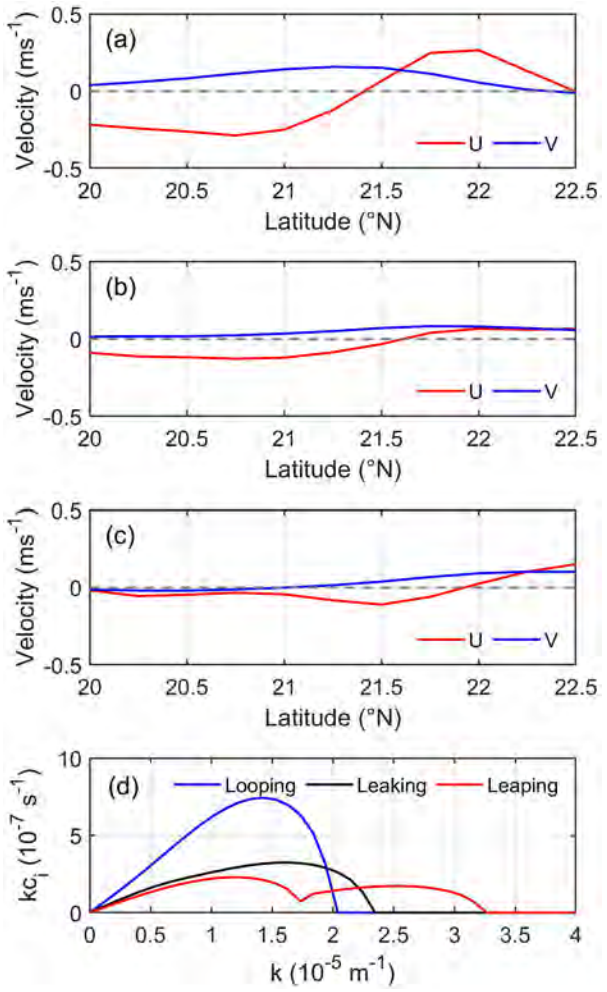

FIG. 14. (a)–(c) Meridional distribution of the surface geostrophic current from 20° to 22.5°N for the looping, leaking, and leaping path of the Kuroshio intrusion, respectively. The velocities are averaged between 118° and 120°E. (d) Growth rates of the unstable waves as a function of zonal wavenumber k associated with the three pathways.

relevant scales for the leaking and leaping paths with a slower growth rate are 61.2 km and 35.7 days and 81.7 km and 50.6 days, respectively. As responses to the surface perturbations, the spectral peaks of BPA around 15 days have been revealed in Fig. 5, whereas those around 30 and 50 days are not significant in the present data but have been observed in the NSCS (Wang et al. 2021; Zheng et al. 2021). Furthermore, according to Quan et al. (2021b, 2023), the theoretical minimum periods of TRWs (related to bottom stratification and slope) and the dominant topographic wavelength in the NSCS are 5–60 days and ~80 km, respectively. This suggests an environmental favor for the rapid growth of SEKE in the Kuroshio intrusion region, as well as the generation and maintenance of TRWs in the abyssal NSCS.

5. Summary

Interactions between the western boundary current and marginal sea are critical to the redistribution and dissipation of global oceanic energy. In this study, the effect of the variable Kuroshio intrusion pathway on the deep flow in the NSCS is investigated using observational and theoretical analyses. With significant seasonality in path variation, the leaking path is found to be most frequent (84.7% for the occurrence probability), whereas the looping (10.7%) and leaping paths (4.6%) are transient and prefer to occur in winter and summer, respectively. Such multipath variability contributes greatly to the highest SEKE in the NSCS, with the energy peaking for the looping path in winter, followed by the leaking and leaping paths. Results of the IF-based causality analysis suggest that the energetic surface perturbations in the Kuroshio intrusion region are causal to the substantial intraseasonal variability in the deep flow east of the Dongsha Islands, wherein the linkage is strongest for the maximum SEKE and BPA observed within the KLCES event related to the looping path. Therefore, the underlying dynamics for the vertical coupling is illustrated by this event, in which the eddy is highly surface intensified because of the sloping topography and the energy is partially transferred downward through vertical pressure work to force the abyssal TRWs. Furthermore, energetics and instability analyses suggest a dominant role for BT in the energy transfer from background flow to eddies in the Kuroshio intrusion region, which energizes the surface perturbations most intensively for the looping path, followed by the leaking and leaping paths. The characteristic scales of the most unstable mode estimated by the reduced-gravity model are analogous to the observations and account for the rapid growth of surface perturbations in the Kuroshio intrusion region.

The observational findings in this study improve our understanding, which is largely based on numerical models, and provide more details about the temporal evolution of the interactions between the Kuroshio and the NSCS. However, several issues remain to be addressed, such as the observation-based evaluation of BT versus BC in the Kuroshio intrusion region and the mechanism for the rapid dissipation of TRWs near the Dongsha Islands. More full-depth observations and high-resolution models are necessary to advance our knowledge of the redistribution and dissipation of energy within the dynamic linkage between the open ocean and the marginal sea.

Acknowledgments. This study is supported by the National Natural Science Foundation of China (42376013, 42276017, 42227901, 42176009, and 42006007), the Natural Science Foundation of Shanghai (23ZR1419100), the Innovation Group Project of Southern Marine Science and Engineering Guangdong Laboratory, Zhuhai (311022001), the Southern Marine Science and Engineering Guangdong Laboratory, Zhuhai (SML2023SP219), and the MEL Visiting Fellowship (MELRS2303). We are grateful to the two anonymous reviewers, Prof. Dake Chen, and Drs. Yu-Kun Qian

and Feng Nan for their insightful comments that improved this manuscript.

Data availability statement. The mooring data are available at http://doi.org/10.6084/m9.figshare.24797076. The satellite data can be accessed from https://resources.marine.copernicus.eu/?option=com_csw&task=results. The *WOA23* and ETOPO1 data are downloaded from https://www.ncei.noaa.gov/products/world-ocean-atlas and https://www.ngdc.noaa.gov/mgg/global/global.html, respectively.

APPENDIX

Modeled Barotropic and Baroclinic Energy Transfer between Background Flow and Eddies in the Kuroshio Intrusion Region of the NSCS

To compare the roles for BT and BC in eddy–mean flow interactions in the Kuroshio intrusion region, we conduct the energetics analysis using the 3-hourly outputs of the Hybrid Coordinate Ocean Model + Navy Coupled Ocean Data Assimilation global 1/12° Analysis (GLBv0.08; https://www.hycom.org/) from 2013 to 2018. Based on the multiscale energy and vorticity analysis (MS-EVA; Liang 2016b), we compute BT and BC between the background flow and eddies. Details of the calculations can be found in Quan et al. (2021a,b, 2022).

The results along the 119°E section of the NSCS are averaged in the data period and are shown in Fig. A1. Consistent with previous studies (Yang et al. 2013; Zhang et al. 2017), the energy transfer between the background flow and eddies in the Kuroshio intrusion region mostly occurs in the upper 1000 m, where BT overwhelms BC. This is similar to theoretical studies (e.g., LaCasce et al. 2019; Palóczy and LaCasce 2022) and numerical studies in the Gulf of Mexico (e.g., Yang et al. 2020; Maslo et al. 2020), which suggest a dominant role for BT in eddy–mean flow interactions over sloping or rough topography.

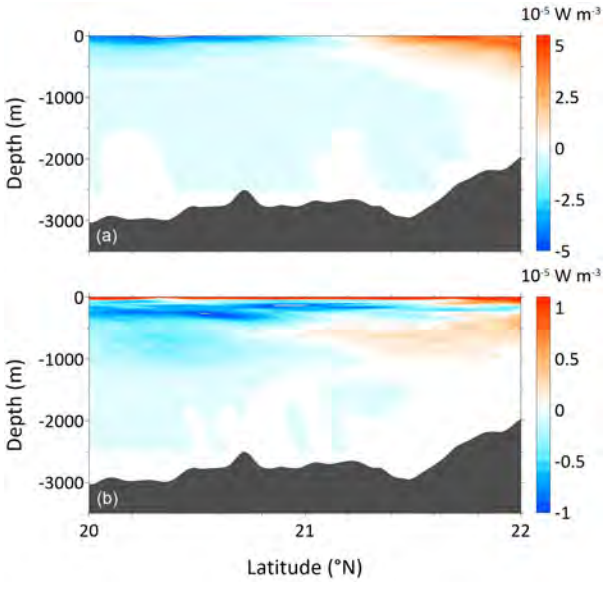

FIG. A1. Vertical profiles of (a) BT and (b) BC along the 119°E section in the Kuroshio intrusion region of the NSCS (yellow rectangle in Fig. 1), based on the GLBv0.08 from 2013 to 2018. Note that the positive values indicate a forward energy cascade from the background flow to eddies, and vice versa.

REFERENCES

Aoki, K., A. Kubokawa, H. Sasaki, and Y. Sasai, 2009: Midlatitude baroclinic Rossby waves in a high-resolution OGCM simulation. *J. Phys. Oceanogr.*, **39**, 2264–2279, https://doi.org/10.1175/2009JPO4137.1.

Chen, G., Y. Hou, and X. Chu, 2011: Mesoscale eddies in the South China Sea: Mean properties, spatiotemporal variability, and impact on thermohaline structure. *J. Geophys. Res.*, **116**, C06018, https://doi.org/10.1029/2010JC006716.

Chen, R., G. R. Flierl, and C. Wunsch, 2014: A description of local and nonlocal eddy–mean flow interaction in a global eddy-permitting state estimate. *J. Phys. Oceanogr.*, **44**, 2336–2352, https://doi.org/10.1175/JPO-D-14-0009.1.

de La Lama, M. S., J. H. LaCasce, and H. K. Fuhr, 2016: The vertical structure of ocean eddies. *Dyn. Stat. Climate Syst.*, **1**, dzw001, https://doi.org/10.1093/climsys/dzw001.

Docquier, D., S. Vannitsem, F. Ragone, K. Wyser, and X. S. Liang, 2022: Causal links between Arctic sea ice and its potential drivers based on the rate of information transfer. *Geophys. Res. Lett.*, **49**, e2021GL095892, https://doi.org/10.1029/2021GL095892.

Donohue, K. A., D. R. Watts, P. Hamilton, R. Leben, and M. Kennelly, 2016: Loop Current eddy formation and baroclinic instability. *Dyn. Atmos. Oceans*, **76**, 195–216, https://doi.org/10.1016/j.dynatmoce.2016.01.004.

Ferrari, R., and C. Wunsch, 2009: Ocean circulation kinetic energy: Reservoirs, sources, and sinks. *Annu. Rev. Fluid Mech.*, **41**, 253–282, https://doi.org/10.1146/annurev.fluid.40.111406.102139.

Gan, J., Z. Liu, and C. Hui, 2016: A three-layer alternating spinning circulation in the South China Sea. *J. Phys. Oceanogr.*, **46**, 2309–2315, https://doi.org/10.1175/JPO-D-16-0044.1.

Hamilton, P., 1990: Deep currents in the Gulf of Mexico. *J. Phys. Oceanogr.*, **20**, 1087–1104, https://doi.org/10.1175/1520-0485(1990)020<1087:DCITGO>2.0.CO;2.

——, 2007: Deep-current variability near the Sigsbee Escarpment in the Gulf of Mexico. *J. Phys. Oceanogr.*, **37**, 708–726, https://doi.org/10.1175/JPO2998.1.

——, 2009: Topographic Rossby waves in the Gulf of Mexico. *Prog. Oceanogr.*, **82** (1), 1–31, https://doi.org/10.1016/j.pocean.2009.04.019.

——, A. Bower, H. Furey, R. Leben, and P. Pérez-Brunius, 2019: The Loop Current: Observations of deep eddies and topographic waves. *J. Phys. Oceanogr.*, **49**, 1463–1483, https://doi.org/10.1175/JPO-D-18-0213.1.

He, Q., H. Zhan, S. Cai, Y. He, G. Huang, and W. Zhan, 2018: A new assessment of mesoscale eddies in the South China Sea: Surface features, three-dimensional structures, and thermohaline transports. *J. Geophys. Res. Oceans*, **123**, 4906–4929, https://doi.org/10.1029/2018JC014054.

Hu, J., H. Kawamura, H. Hong, and Y. Qi, 2000: A review on the currents in the South China Sea: Seasonal circulation, South China Sea Warm Current and Kuroshio intrusion. *J. Oceanogr.*, **56**, 607–624, https://doi.org/10.1023/A:1011117531252.

Huang, Z., H. Liu, J. Hu, and P. Lin, 2016: A double-index method to classify Kuroshio intrusion paths in the Luzon Strait. *Adv. Atmos. Sci.*, **33**, 715–729, https://doi.org/10.1007/s00376-015-5171-y.

Hurlburt, H. E., and J. D. Thompson, 1980: A numerical study of Loop Current intrusions and eddy shedding. *J. Phys. Oceanogr.*, **10**, 1611–1651, https://doi.org/10.1175/1520-0485(1980)010<1611:ANSOLC>2.0.CO;2.

Jönsson, B., K. Döös, and J. Kjellsson, 2015: TRACMASS: Lagrangian trajectory code. Zenodo, accessed 27 August 2024, https://doi.org/10.5281/zenodo.34157.

LaCasce, J. H., 2017: The prevalence of oceanic surface modes. *Geophys. Res. Lett.*, **44**, 11 097–11 105, https://doi.org/10.1002/2017GL075430.

——, and S. Groeskamp, 2020: Baroclinic modes over rough bathymetry and the surface deformation radius. *J. Phys. Oceanogr.*, **50**, 2835–2847, https://doi.org/10.1175/JPO-D-20-0055.1.

——, J. Escartin, E. P. Chassignet, and X. Xu, 2019: Jet instability over smooth, corrugated, and realistic bathymetry. *J. Phys. Oceanogr.*, **49**, 585–605, https://doi.org/10.1175/JPO-D-18-0129.1.

Liang, X. S., 2008: Information flow within stochastic dynamical systems. *Phys. Rev.*, **78E**, 031113, https://doi.org/10.1103/PhysRevE.78.031113.

——, 2014: Unraveling the cause-effect relation between time series. *Phys. Rev.*, **90E**, 052150, https://doi.org/10.1103/PhysRevE.90.052150.

——, 2015: Normalizing the causality between time series. *Phys. Rev.*, **92E**, 022126, https://doi.org/10.1103/PhysRevE.92.022126.

——, 2016a: Information flow and causality as rigorous notions *ab initio*. *Phys. Rev.*, **94E**, 052201, https://doi.org/10.1103/PhysRevE.94.052201.

——, 2016b: Canonical transfer and multiscale energetics for primitive and quasigeostrophic atmospheres. *J. Atmos. Sci.*, **73**, 4439–4468, https://doi.org/10.1175/JAS-D-16-0131.1.

——, and R. Kleeman, 2005: Information transfer between dynamical system components. *Phys. Rev. Lett.*, **95**, 244101, https://doi.org/10.1103/PhysRevLett.95.244101.

——, and A. R. Robinson, 2007: Localized multi-scale energy and vorticity analysis: II. Finite-amplitude instability theory and validation. *Dyn. Atmos. Oceans*, **44**, 51–76, https://doi.org/10.1016/j.dynatmoce.2007.04.001.

Liu, D., Y. Shu, D. Wang, W. Wang, T. Zu, and W. Zhou, 2023: Effect of western Pacific current uncertainties on the forecasting of eddy shedding from the Kuroshio loop into the South China Sea: A case study. *Ocean Modell.*, **184**, 102234, https://doi.org/10.1016/j.ocemod.2023.102234.

Maslo, A., J. M. A. C. De Souza, and J. S. Pardo, 2020: Energetics of the deep Gulf of Mexico. *J. Phys. Oceanogr.*, **50**, 1655–1675, https://doi.org/10.1175/JPO-D-19-0308.1.

Mei, H., K. Li, Q. Liu, B. Wang, and X. Wu, 2023: Interaction of a hysteresis western boundary current with a large-scale marginal sea circulation in a gap-leaping system. *J. Phys. Oceanogr.*, **53**, 943–957, https://doi.org/10.1175/JPO-D-22-0194.1.

Nan, F., 2012: Spatiotemporal evolution of the current-eddy structure southwest of Taiwan (in Chinese with English abstract). Ph.D. thesis, Ocean University of China, 119 pp.

——, H. Xue, F. Chai, L. Shi, M. Shi, and P. Guo, 2011a: Identification of different types of Kuroshio intrusion into the South China Sea. *Ocean Dyn.*, **61**, 1291–1304, https://doi.org/10.1007/s10236-011-0426-3.

——, ——, P. Xiu, F. Chai, M. Shi, and P. Guo, 2011b: Oceanic eddy formation and propagation southwest of Taiwan. *J. Geophys. Res.*, **116**, C12045, https://doi.org/10.1029/2011JC007386.

——, ——, and F. Yu, 2015: Kuroshio intrusion into the South China Sea: A review. *Prog. Oceanogr.*, **137**, 314–333, https://doi.org/10.1016/j.pocean.2014.05.012.

Ni, Q., X. Zhai, J. H. LaCasce, D. Chen, and D. P. Marshall, 2023: Full-depth eddy kinetic energy in the global ocean estimated from altimeter and Argo observations. *Geophys. Res. Lett.*, **50**, e2023GL103114, https://doi.org/10.1029/2023GL103114.

Oey, L.-Y., 1996: Simulation of mesoscale variability in the Gulf of Mexico: Sensitivity studies, comparison with observation, and trapped waves propagation. *J. Phys. Oceanogr.*, **26**, 145–175, https://doi.org/10.1175/1520-0485(1996)026<0145:SOMVIT>2.0.CO;2.

——, 2008: Loop Current and deep eddies. *J. Phys. Oceanogr.*, **38**, 1426–1449, https://doi.org/10.1175/2007JPO3818.1.

——, and H.-C. Lee, 2002: Deep eddy energy and topographic Rossby waves in the Gulf of Mexico. *J. Phys. Oceanogr.*, **32**, 3499–3527, https://doi.org/10.1175/1520-0485(2002)032<3499:DEEATR>2.0.CO;2.

Palóczy, A., and J. H. LaCasce, 2022: Instability of a surface jet over rough topography. *J. Phys. Oceanogr.*, **52**, 2725–2740, https://doi.org/10.1175/JPO-D-22-0079.1.

Qiu, B., and S. Chen, 2004: Seasonal modulations in the eddy field of the South Pacific Ocean. *J. Phys. Oceanogr.*, **34**, 1515–1527, https://doi.org/10.1175/1520-0485(2004)034<1515:SMITEF>2.0.CO;2.

Qu, T., 2000: Upper-layer circulation in the South China Sea. *J. Phys. Oceanogr.*, **30**, 1450–1460, https://doi.org/10.1175/1520-0485(2000)030<1450:ULCITS>2.0.CO;2.

Quan, Q., Z. Liu, S. Sun, Z. Cai, Y. Yang, G. Jin, Z. Li, and X. S. Liang, 2021a: Influence of the Kuroshio intrusion on deep flow intraseasonal variability in the northern South China Sea. *J. Geophys. Res. Oceans*, **126**, e2021JC017429, https://doi.org/10.1029/2021JC017429.

——, Z. Cai, G. Jin, and Z. Liu, 2021b: Topographic Rossby waves in the abyssal South China Sea. *J. Phys. Oceanogr.*, **51**, 1795–1812, https://doi.org/10.1175/JPO-D-20-0187.1.

——, Z. Liu, Y. Yang, Z. Cai, H. Zhang, and X. Liu, 2022: Characterization of intraseasonal fluctuations in the abyssal South China Sea: An insight into the energy pathway. *Prog. Oceanogr.*, **206**, 102829, https://doi.org/10.1016/j.pocean.2022.102829.

——, and Coauthors, 2023: Observed oceanic surface modes in the northern South China Sea. *J. Phys. Oceanogr.*, **53**, 1835–1849, https://doi.org/10.1175/JPO-D-22-0250.1.

Sheremet, V. A., 2001: Hysteresis of a western boundary current leaping across a gap. *J. Phys. Oceanogr.*, **31**, 1247–1259, https://doi.org/10.1175/1520-0485(2001)031<1247:HOAWBC>2.0.CO;2.

Shu, Y., Q. Wang, and T. Zu, 2018: Progress on shelf and slope circulation in the northern South China Sea. *Sci. China Earth Sci.*, **61**, 560–571, https://doi.org/10.1007/s11430-017-9152-y.

——, and Coauthors, 2022: Deep-current intraseasonal variability interpreted as topographic Rossby waves and deep eddies in the Xisha Islands of the South China Sea. *J. Phys. Oceanogr.*, **52**, 1415–1430, https://doi.org/10.1175/JPO-D-21-0147.1.

Stewart, A. L., P. J. Dellar, and E. R. Johnson, 2011: Numerical simulation of wave propagation along a discontinuity in depth in a rotating annulus. *Comput. Fluids*, **46**, 442–447, https://doi.org/10.1016/j.compfluid.2010.10.016.

Sun, Z., J. Hu, Z. Chen, J. Zhu, L. Yang, X. Chen, and X. Wu, 2021: A strong Kuroshio intrusion into the South China Sea and its accompanying cold-core anticyclonic eddy in winter

2020–2021. *Remote Sens.*, **13**, 2645, https://doi.org/10.3390/rs13142645.

Tailleux, R., and J. C. McWilliams, 2001: The effect of bottom pressure decoupling on the speed of extratropical, baroclinic Rossby waves. *J. Phys. Oceanogr.*, **31**, 1461–1476, https://doi.org/10.1175/1520-0485(2001)031<1461:TEOBPD>2.0.CO;2.

Tenreiro, M., J. Candela, E. P. Sanz, J. Sheinbaum, and J. Ochoa, 2018: Near-surface and deep circulation coupling in the western Gulf of Mexico. *J. Phys. Oceanogr.*, **48**, 145–161, https://doi.org/10.1175/JPO-D-17-0018.1.

Wang, D., Q. Liu, R. X. Huang, Y. Du, and T. Qu, 2006: Interannual variability of the South China Sea throughflow inferred from wind data and an ocean data assimilation product. *Geophys. Res. Lett.*, **33**, L14605, https://doi.org/10.1029/2006GL026316.

Wang, G., D. Chen, and J. Su, 2008: Winter eddy genesis in the eastern South China Sea due to orographic wind jets. *J. Phys. Oceanogr.*, **38**, 726–732, https://doi.org/10.1175/2007JPO3868.1.

Wang, J., Y. Shu, D. Wang, Q. Xie, Q. Wang, J. Chen, T. Zu, D. Liu, and Y. He, 2021: Observed variability of bottom-trapped topographic Rossby waves along the slope of the northern South China Sea. *J. Geophys. Res. Oceans*, **126**, e2021JC017746, https://doi.org/10.1029/2021JC017746.

Wang, Q., and Coauthors, 2019: Energetic topographic Rossby waves in the northern South China Sea. *J. Phys. Oceanogr.*, **49**, 2697–2714, https://doi.org/10.1175/JPO-D-18-0247.1.

——, L. Zeng, J. Chen, Y. He, W. Zhou, and D. Wang, 2020a: The linkage of Kuroshio intrusion and mesoscale eddy variability in the northern South China Sea: Subsurface speed maximum. *Geophys. Res. Lett.*, **47**, e2020GL087034, https://doi.org/10.1029/2020GL087034.

——, W. Zhou, L. Zeng, J. Chen, Y. He, and D. Wang, 2020b: Intraseasonal variability of cross-slope flow in the northern South China Sea. *J. Phys. Oceanogr.*, **50**, 2071–2084, https://doi.org/10.1175/JPO-D-19-0293.1.

Wang, Y., and A. L. Stewart, 2018: Eddy dynamics over continental slopes under retrograde winds: Insights from a model inter-comparison. *Ocean Modell.*, **121**, 1–18, https://doi.org/10.1016/j.ocemod.2017.11.006.

Weisberg, R. H., and Y. Liu, 2017: On the Loop Current penetration into the Gulf of Mexico. *J. Geophys. Res. Oceans*, **122**, 9679–9694, https://doi.org/10.1002/2017JC013330.

Wu, C.-R., 2013: Interannual modulation of the Pacific Decadal Oscillation (PDO) on the low-latitude western North Pacific. *Prog. Oceanogr.*, **110**, 49–58, https://doi.org/10.1016/j.pocean.2012.12.001.

——, and Y.-C. Hsin, 2012: The forcing mechanism leading to the Kuroshio intrusion into the South China Sea. *J. Geophys. Res.*, **117**, C07015, https://doi.org/10.1029/2012JC007968.

——, Y.-L. Wang, Y.-F. Lin, and S.-Y. Chao, 2017: Intrusion of the Kuroshio into the South and East China Seas. *Sci. Rep.*, **7**, 7895, https://doi.org/10.1038/s41598-017-08206-4.

Wunsch, C., 1997: The vertical partition of oceanic horizontal kinetic energy. *J. Phys. Oceanogr.*, **27**, 1770–1794, https://doi.org/10.1175/1520-0485(1997)027<1770:TVPOOH>2.0.CO;2.

——, and R. Ferrari, 2004: Vertical mixing, energy, and the general circulation of the oceans. *Annu. Rev. Fluid Mech.*, **36**, 281–314, https://doi.org/10.1146/annurev.fluid.36.050802.122121.

Xu, F.-H., and L.-Y. Oey, 2015: Seasonal SSH variability of the northern South China Sea. *J. Phys. Oceanogr.*, **45**, 1595–1609, https://doi.org/10.1175/JPO-D-14-0193.1.

——, Y.-L. Chang, L.-Y. Oey, and P. Hamilton, 2013: Loop Current growth and eddy shedding using models and observations: Analyses of the July 2011 eddy-shedding event. *J. Phys. Oceanogr.*, **43**, 1015–1027, https://doi.org/10.1175/JPO-D-12-0138.1.

Xue, H., F. Chai, N. Pettigrew, D. Xu, M. Shi, and J. Xu, 2004: Kuroshio intrusion and the circulation in the South China Sea. *J. Geophys. Res.*, **109**, C02017, https://doi.org/10.1029/2002JC001724.

Yang, H., L. Wu, H. Liu, and Y. Yu, 2013: Eddy energy sources and sinks in the South China Sea. *J. Geophys. Res. Oceans*, **118**, 4716–4726, https://doi.org/10.1002/jgrc.20343.

Yang, Y., R. H. Weisberg, Y. Liu, and X. S. Liang, 2020: Instabilities and multiscale interactions underlying the Loop Current eddy shedding in the Gulf of Mexico. *J. Phys. Oceanogr.*, **50**, 1289–1317, https://doi.org/10.1175/JPO-D-19-0202.1.

——, G. Fu, X. S. Liang, R. H. Weisberg, and Y. Liu, 2023: Causal relations between the Loop Current penetration and the inflow/outflow conditions inferred with a rigorous quantitative causality analysis. *Deep-Sea Res. II*, **209**, 105298, https://doi.org/10.1016/j.dsr2.2023.105298.

Yassin, H., and S. M. Griffies, 2022: On the discrete normal modes of quasigeostrophic theory. *J. Phys. Oceanogr.*, **52**, 243–259, https://doi.org/10.1175/JPO-D-21-0199.1.

Yuan, D., and Z. Wang, 2011: Hysteresis and dynamics of a western boundary current flowing by a gap forced by impingement of mesoscale eddies. *J. Phys. Oceanogr.*, **41**, 878–888, https://doi.org/10.1175/2010JPO4489.1.

——, W. Han, and D. Hu, 2006: Surface Kuroshio path in the Luzon Strait area derived from satellite remote sensing data. *J. Geophys. Res.*, **111**, C11007, https://doi.org/10.1029/2005JC003412.

Zhai, X., and D. P. Marshall, 2013: Vertical eddy energy fluxes in the North Atlantic subtropical and subpolar gyres. *J. Phys. Oceanogr.*, **43**, 95–103, https://doi.org/10.1175/JPO-D-12-021.1.

Zhang, Z., W. Zhao, B. Qiu, and J. Tian, 2017: Anticyclonic eddy sheddings from Kuroshio Loop and the accompanying cyclonic eddy in the northeastern South China Sea. *J. Phys. Oceanogr.*, **47**, 1243–1259, https://doi.org/10.1175/JPO-D-16-0185.1.

Zhao, Y., X. S. Liang, and Y. Yang, 2023: The Kuroshio intrusion into the South China Sea at Luzon Strait can be remotely influenced by the downstream intrusion into the East China Sea. *J. Geophys. Res. Oceans*, **128**, e2023JC019868, https://doi.org/10.1029/2023JC019868.

Zheng, H., X.-H. Zhu, C. Zhang, R. Zhao, Z.-N. Zhu, and Z.-J. Liu, 2021: Propagation of topographic Rossby waves in the deep basin of the South China Sea based on abyssal current observations. *J. Phys. Oceanogr.*, **51**, 2783–2791, https://doi.org/10.1175/JPO-D-21-0051.1.

Zhu, Y. H., J. Sun, Y. Wang, Z. Wei, D. Yang, and T. Qu, 2017: Effect of potential vorticity flux on the circulation in the South China Sea. *J. Geophys. Res. Oceans*, **122**, 6454–6469, https://doi.org/10.1002/2016JC012375.

Zhu, Y. L., and X. Liang, 2020: Coupling of the surface and near-bottom currents in the Gulf of Mexico. *J. Geophys. Res. Oceans*, **125**, e2020JC016488, https://doi.org/10.1029/2020JC016488.